Pavement design method in Japan with consideration of climate effect and principal stress axis rotation

Tianshu Lin [a], Tatsuya Ishikawa [b*], Kimio Maruyama [c], Tetsuya Tokoro [d]

[a] Graduate School of Engineering, Hokkaido University, Kita 13, Nishi 8, Kita-Ku, Sapporo 060-8628, Japan

[b] Faculty of Engineering, Hokkaido University, Kita 13, Nishi 8, Kita-Ku, Sapporo 060-8628, Japan

[c] Cold-Region Maintenance Engineering Research Group, Civil Engineering Research Institute for Cold Region, 1-34, Hiragishi 1, 3, Toyohira-ku, Sapporo 062-8602, Japan

[d] Faculty of Engineering, Hokkai-Gakuen University, 1-1, Minami 26 Nishi 11, Chuo-ku, Sapporo 064-0926, Japan

Key words

Rutting; Fatigue cracking; Freeze-thaw action; Resilient modulus; Mechanical-empirical design method

Abstract

Current Japanese design guide uses mechanical-empirical criteria to predict the failure loading number against fatigue cracking and rutting. However, these criteria have some limitations that

[*] Corresponding author. Email address: t-ishika@eng.hokudai.ac.jp

the variation in moduli of base and subgrade layer due to the fluctuation in water contents, freeze-thaw history, and stress states are not considered. As well known, these factors greatly affect the soil mechanical properties like resilient modulus. Besides, present rutting failure criterion provides no indication of the behavior of rutting over time, and the effect of principal stress axis rotation on rutting development is also not captured. To overcome such limitations, this study modified the present Japanese pavement design method through the following two main aspects: (1) Replacing constant elastic modulus of base and subgrade layer to resilient modulus related to stress states and complex climate conditions, which are defined as the combination of fluctuating water content and freeze-thaw action; (2) Modifying rutting failure criterion by considering generally used MEPDG model and also the effect of principal stress axis rotation. All modifications are performed based on laboratory element test like suction-controlled freeze-thaw triaxial test, which could simulate complex climate conditions, and multi-ring shear test, which could simulate principal stress axis rotation. Besides, modified criteria are examined by comparing to long-term measured performance of test pavements built in Hokkaido, the north island of Japan. Modified Japanese pavement design method shows high applicability and accuracy on the pavement life prediction, especially for the flexible pavement in cold regions like Hokkaido.

1. Introduction

Mechanistic-Empirical Pavement Design Guide (MEPDG), which combines empirical and mechanistic concepts, uses input data such as materials, traffic, climate, and for a trial design calculates mechanistically stresses and strains, which are subsequently used in empirical distress models to compute damage accumulated over time like rutting, fatigue cracking, and thermal cracking. MEPDG has been mainly used in the United States. At the current time with regard to Japan, a mechanistic-empirical method based only on a multi-layer linear elastic model is still currently being used and as a consequence, the applicability and prediction precision are unsatisfactory.

To be previse, several serious drawbacks limit the applicability and accuracy of present Japanese pavement design method. First, constant base and subgrade layer moduli through the whole year based on linear elastic theory restrict the precision since soil shows nonlinear elastic property in small strain period as reviewed by Clayton [2011]. Based on such nonlinearity, resilient modulus (M_r) is proposed [Seed, 1955] to capture the effect of stress states on the stiffness of soil. M_r is widely used in Mechanistic-Empirical Pavement Design Guide (MEPDG) and estimated by Eq. (1), named as the universal model [AASHTO, 2008]. According to Eq. (1), the resilient modulus decreases with increasing deviator stress and decreasing confining pressure. In general, based on laboratory element test results, resilient modulus of base course and subgrade material are determined and employed as the layer moduli in a multi-layered elastic pavement response model.

$$M_r = k_1 p_a \left(\frac{\theta}{p_a}\right)^{k_2} \left(\frac{\tau_{oct}}{p_a} + 1\right)^{k_3} \qquad (1)$$

where k_1, k_2, k_3 are regression constants; p_a is atmospheric pressure and set as 101 kPa in this study; θ is bulk stress (kPa); τ_{oct} is octahedral stress (kPa).

Second, effects of water content and freeze-thaw action, which greatly influence the stiffness of base and subgrade layer [Berg et al., 1996; Cole et al., 1981; Johnson et al., 1978; Simonsen et al., 2002; Simonsen and Isacsson, 2001], are not considered in Japanese pavement design method.

To be precise, rising water content, as a result of the inflow of water during rainfall or the thawing of ice lenses, causes a temporary decrease in the stiffness of base course and subgrade materials. Meanwhile, freeze-thaw action always decreases moduli of base and subbase layer materials even with no excess water storage after thawing [Ishikawa et al., 2019a; Lin et al., 2019b], as ice formation tends to break some of the particle contacts and interlocking of soil particles and finally deteriorates the soil structure uniformity and stiffness.

Third, current rutting model cannot capture the behavior of rutting over time or with the application of traffic loading. It also does not consider rate-hardening or the contribution of the non-subgrade layers to rutting. To overcome these limitations, MEPDG proposed a rutting depth prediction model [NCHRP, 2004], which converts the plastic strain measured from the laboratory to the field condition, as shown in Eq. (2).

$$\varepsilon_p(N) = \beta_1 k_1 (\frac{\varepsilon_0}{\varepsilon_r}) e^{-(\frac{\rho}{N})^{\beta}} \varepsilon_v \tag{2}$$

where $\varepsilon_p(N)$ is permanent strain for the layer/sub-layer; N is number of traffic repetitions; ε_0, β, and ρ are material properties; ε_r is resilient strain imposed in laboratory test to obtain material properties ε_0, β, and ρ; ε_v is average vertical resilient strain in the layer, which is calculated by a multi-layer elastic pavement response model; β_1 is calibration factor for the unbound granular and subgrade materials; k_1 is global calibration coefficients.

Last, the rutting failure criterion in Japanese pavement design guide as well as MEPDG rutting model does not capture the effect of principal stress axis rotation (PSAR), which is a phenomenon caused by moving wheel loads and greatly amplifies the permanent deformation of base and subgrade layer [Miura et al., 1986; Brown, 1996; Gräbe and Clayton, 2009; Inam et al., 2012; Ishikawa et al., 2011, 2019b; Lin et al., 2019a]. This is because the conventional rutting models are mainly built on traditional repeated loading triaxial test with constant confining pressure and no principal stress axis rotation.

Consequently, to overcome aforementioned limitations, this study modified the present Japanese pavement design method through two main aspects: (1) Replacing constant elastic modulus of base and subgrade layer to resilient modulus related to stress states and complex climate conditions, which are defined as the combination of fluctuating water content and freeze-thaw action. To be precise, Ishikawa et al. [2019a] and Lin et al. [2020] studied the synergistic effect between water content and freeze-thaw action, named as climate effect, on the base course and subgrade materials. This study combined these research results to determine the base and subgrade layer moduli with complex water content and freeze-thaw conditions. (2) Modifying rutting failure criterion by considering generally used MEPDG model and also the effect of principal stress axis rotation. To be precise, this study modified the structure of present rutting model referring to MEPDG rutting model. Furthermore, the amplification of permanent deformation caused by PSAR is examined through laboratory test results. Such effect caused by PSAR was also used to modify the structure of rutting failure criterion in this study. This study specially focuses on the pavement life against rutting since modification of the fatigue cracking model is done by previous researches [Maruyama et al., 2006, 2008].

2. Applicability of present Japanese pavement design method

2.1 Present Japanese pavement design method

Japanese pavement design method [JRA, 2006] provides rutting and fatigue cracking failure criteria, as shown in Eqs. (3) to (5) and (6) to (13), to calculate allowable loading number of equivalent 49-kN wheel loads against rutting (N_{fs}) and fatigue cracking (N_{fa}). These allowable loading numbers are calculated by a theoretical design method, also known as AI model, [Asphalt Institute, 1982] using a simplified three-layers model which consists of asphalt mixture layer (hereafter referred to as the "As layer"), base layer, and subgrade layer as shown in Fig. 1.

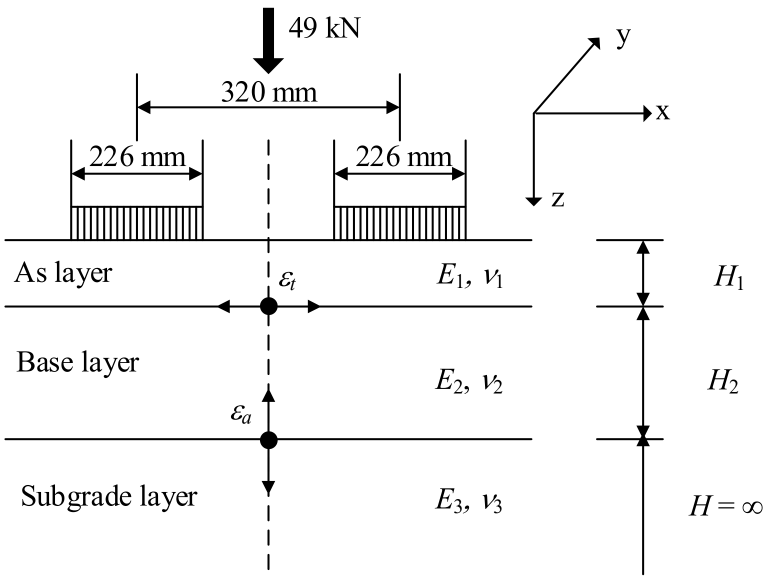

Fig. 1 Three-layers model for allowable loading number calculation.

$$N_{fs} = \beta_{s1} \cdot \{1.365 \times 10^{-9} \cdot {\varepsilon_a}^{-4.477 \cdot \beta_{s2}}\} \tag{3}$$

$$\beta_{s1} = 2134 \tag{4}$$

$$\beta_{s2} = 0.819 \tag{5}$$

$$N_{fa} = \beta_{a1} \cdot C \cdot \{6.167 \times 10^{-5} \cdot {\varepsilon_t}^{-3.291 \cdot \beta_{a2}} \cdot {E_1}^{-0.854 \cdot \beta_{a3}}\} \tag{6}$$

$$C = 10^M \tag{7}$$

$$M = 4.84 * \left(\frac{VFA}{100} - 0.69\right) \tag{8}$$

$$\beta_{a1} = K_a * {\beta_{a1}}' \tag{9}$$

$$K_a = \begin{cases} \frac{1}{8.27\times10^{-11}+7.83\cdot e^{-0.11H_a}}, & H_1 < 0 \\ 1, & H_1 \geq 0 \end{cases} \quad (10)$$

$$\beta_{a1}' = 5.229 \times 10^4 \quad (11)$$

$$\beta_{a2} = 1.314 \quad (12)$$

$$\beta_{a3} = 3.018 \quad (13)$$

where β_{s1}, β_{s2}, β_{a1}, β_{a2}, and β_{a3} are the compensation rates for AI failure criteria based on the actual situation of Japanese pavement; C is the material parameter; M is a factor relates the VFA to C; VFA is Voids Filled with Asphalt; K_a is a correction factor, which relates to the thickness of asphalt mixture, H_1. ε_a is the compressive strain on the top surface of the subgrade layer; ε_t is the tensile strain on the lower surface of the As layer.

ε_a and ε_t are determined through multi-layers model, which involves elastic moduli (E) and Poisson's ratio (v) of each layer, built in General Analysis of Multi-layered Elastic Systems (GAMES) [Maina and Matsui, 2004] as shown in Fig 1. In present Japanese pavement design method, elastic moduli of As layer (E_1) changes with temperature as shown in Eqs. (14) and (15), while the elastic moduli of base layer (E_2) and subgrade layers (E_3) are constant throughout a whole year since lacking investigation of how water content, freeze-thaw, or stress states influence E_2 and E_3.

$$E_1 = -278.4M_p + 10930 \quad (14)$$

$$M_p = M_a\left[1 + \frac{2.54}{h_1+10.16}\right] - \frac{25.4}{9(h_1+10.16)} + \frac{10}{3} \quad (15)$$

where M_p is the monthly mean temperature of asphalt mixture at depth of h_1 (°C); M_a is monthly mean air temperature (°C); h_1 is the depth equals to one-third of the height of asphalt mixture (cm).

Consequently, monthly representative E_1 and constant E_2/E_3 are used to calculate allowable loading number under monthly average temperature condition, $N_{fs.i}$ and $N_{fa.i}$. i=1~12. Failure loading number $N_{fs.d}$ or $N_{fa.d}$ is calculated through Eqs. (16) and (17).

$$N_{f.d} = \frac{1}{D_a} \tag{16}$$

$$D_a = \frac{1}{12}\sum_{i=1}^{12}\frac{1}{N_{f.i}} \tag{17}$$

As a result, Fig. 2 illustrates the sequence in current Japanese flexible pavement design guide.

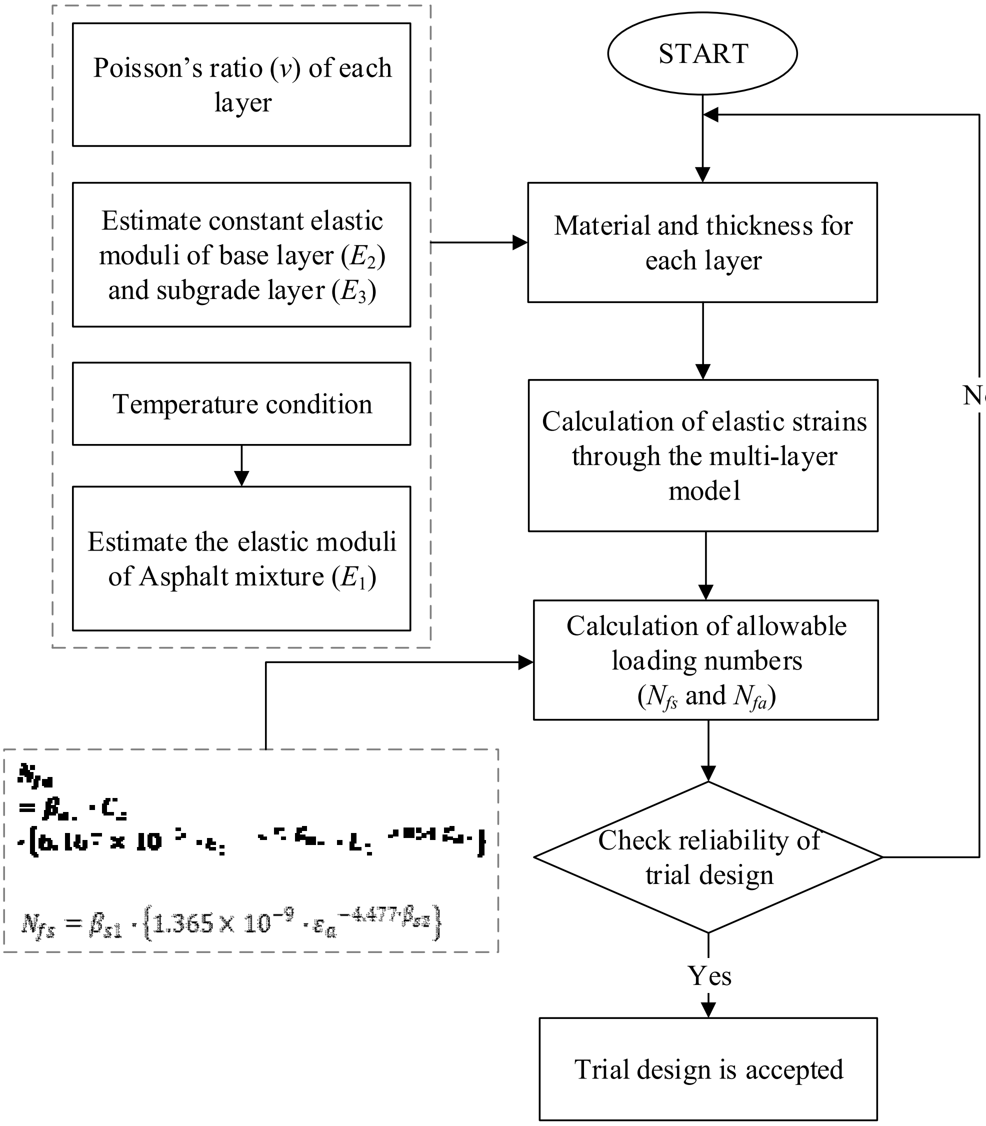

Fig. 2 Sequence in current Japanese flexible pavement design guide.

2.2 Test pavement structures

Civil Engineering Research Institute for Cold Region (CERI) designed and constructed eight test pavements in Hokkaido [Maruyama et al., 2006]. Fig. 3 illustrates the structures and length of each test pavement. All eight pavement structures consist of asphalt mixture, base layer, and subgrade layer with multiple materials and thickness. Four types of hot mixed asphalt mixtures are used in test pavement. Fine-graded asphalt mixture has a 0 - 13 mm aggregate gradation distribution (hydrated lime, sea sand, and crushed rock). Middle-graded asphalt mixture has the same range of gradation distribution but more coarse aggregate. Coarse-graded and stabilized asphalt mixture have a 0 - 20 mm and 0 - 30 mm gradation distribution separately. Two types of base layer material (Andesite) are used as C-40, crusher-run with maximum 40 mm gradation distribution, and C-80, anti-frost crusher-run with maximum 80 mm gradation distribution. The subgrade material is a sandy soil according to Unified Soil Classification System [ASTM, 2011], named as Tomakomai soil, composed of 8% clay, 13% silt, 51% sand, 28% gravel.

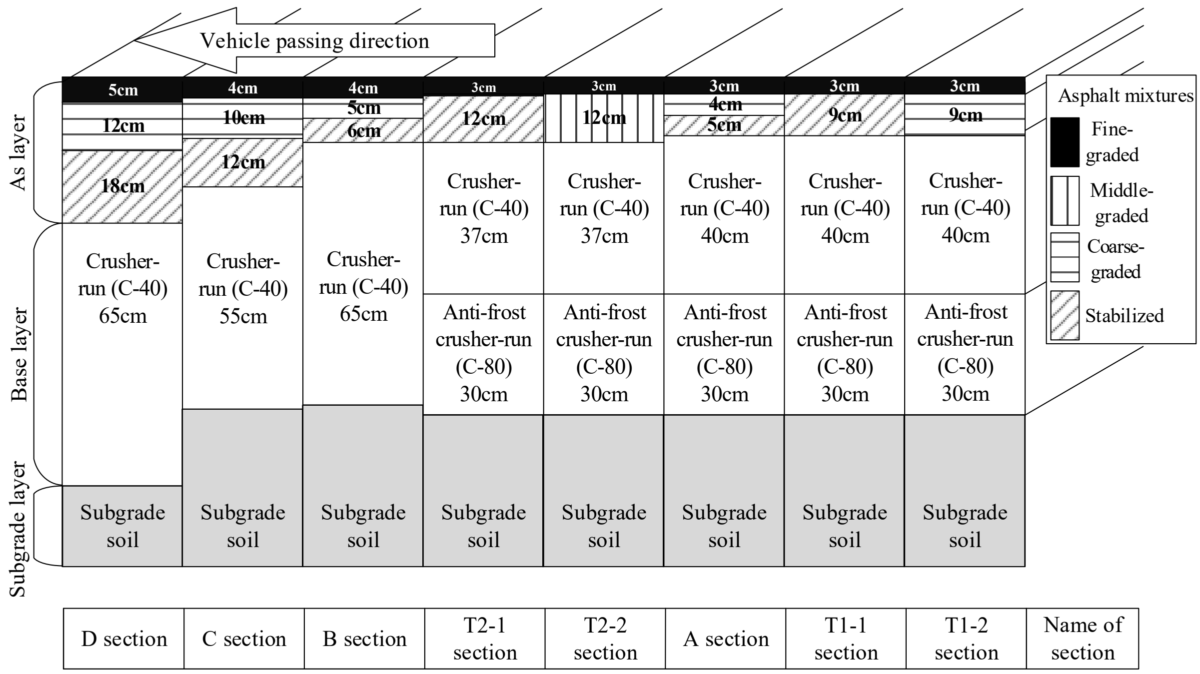

Fig. 3 Test pavement structures.

2.3 Traffic volume observation

CERI observed traffic volume of test pavement during the whole life (from 1990 to 2004). Total traffic volume, that is average annual daily vehicle (car and truck) number in one lane, is 4974 per day per lane. Truck volume, that is average annual daily truck number in one lane, is 1714 per day per lane. Wheel loads for all vehicles are in accordance with the normal distribution that ranges from 15 to 80 kN. As Japanese pavement design method calculates the allowable number of equivalent 49-kN wheel loads against rutting and fatigue cracking. CERI transferred the traffic volume to a 49-kN wheel loads number as 2398 per day per lane during the whole life of test pavement.

2.4 Climate data

Climate data are collected from Automated Meteorological Data Acquisition System (AMeDAS) [Japan Meteorological Agency]. Fig. 4 plots the monthly average value of daily temperatures during the whole life from 1990 to 2004. These climate data are used to determine the stiffness of the asphalt layer in current Japanese pavement design method through Eqs. (14) and (15). Besides, the monthly representative temperature is also used in modified design method to determine the frost-penetration depth, which highly relates to the stiffness of base and subgrade layer as frozen soil has a much larger stiffness. Determination of variant base and subgrade layer stiffness related to climate condition will be introduced in latter part.

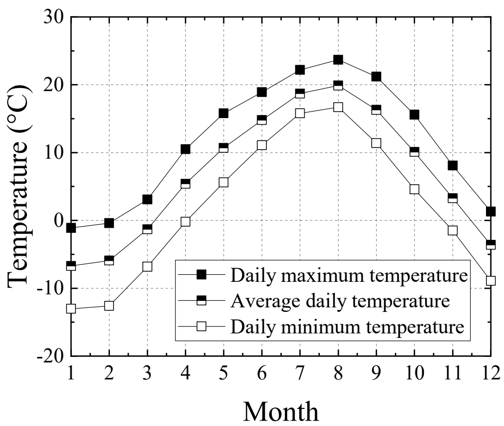

Fig. 4 Monthly average value of daily temperatures.

2.5 Predicted life with present Japanese pavement design method

To predict the life of eight test pavements, all test pavements are simplified to three-layers model in GAMES with layer thickness shown in Fig. 3. E_1 is determined through Eqs. (14) and (15) and monthly representative air temperatures shown in Fig. 4. Constant stiffness of base layer (E_2) and subgrade layer (E_3) through the year is set as 265MPa and 76 MPa referring to previous research [Maruyama et al., 2008]. Poisson's ratio of As layer, base layer, and subgrade layer are set as 0.35, 0.35, and 0.4 separately, which come from Japanese pavement design method recommend values. Fig. 5 compared predicted N_{fs} and N_{fa} through Eqs. (3) to (5) and (6) to (13) with actual measured failure loading number. From Fig.5, it is recognized that, present AI model over-estimates the pavement life, especially pavement life against rutting. Besides, prediction bias is much larger for pavement structures with thick As layer refer to two dots circled by dash line in Fig. 5. Such over-estimation is attributed to the drawbacks of Japanese pavement design method discussed in Introduction part.

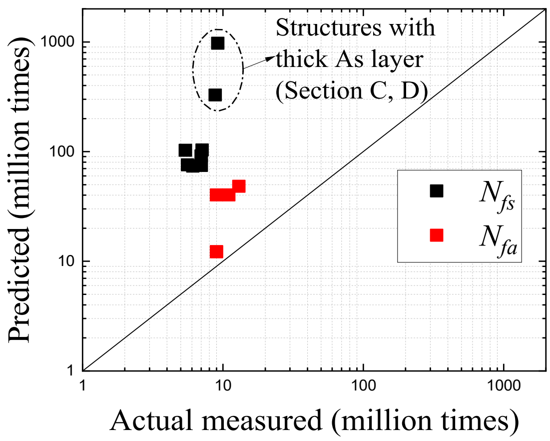

Fig. 5 Predicted pavement life through present Japanese pavement design method.

3. Resilient modulus under various climate conditions and different stress states

3.1 Climate effect on resilient modulus

3.1.1 Water content fluctuation

Climate effect in this study refers to the synergistic effect between water content and freeze-thaw action on the resilient modulus of base course and subgrade materials and pavement life. The universal model (Eq. (1)) cannot reflect the effect of water content. To overcome such shortcoming, several modified models [Cary and Zapata, 2011; Liang et al., 2008; Ng et al., 2013] are proposed based on the universal model to capture the effect of water content on resilient modulus. Within these models, Ng model shown in Eq. (18) adds an independent stress state variable that incorporates matric suction effects into the universal model and shows good applicability on predicting resilient modulus of unsaturated unbound granular materials through the relatively higher coefficient of determination (R^2) value than other models [Han and Vanapalli, 2016]. Monthly representative E_2 and E_3 are estimated through Ng model (Eq. (18)), field-measured data of water content, and SWCC of base course material and subgrade material.

$$M_r = k_1 p_a \left(\frac{\theta}{p_a}\right)^{k_2} \left(\frac{\tau_{oct}}{p_a} + 1\right)^{k_3} \left(\frac{\psi}{\sigma_{net}} + 1\right)^{k_4} \tag{18}$$

where k_1, k_2, k_3, k_4 are regression constants; p_a is atmospheric pressure and set as 101 kPa; θ is bulk stress; τ_{oct} is octahedral shear stress; σ_{net} is net mean stress (kPa), defined as $[\theta/3-u_a]$; ψ is matric suction (kPa).

Matric suction, ψ in Eq. (18), is determined by combining SWCC and measured long-term field measurement of degree of saturation. SWCC of C-40, composed material for base layer, and long-term field measured water content of base layer are plotted in Fig. 6. The effective degree of saturation, S_e, of base layer illustrated as the red line in Fig. 6 (a) was calculated by using a residual degree of saturation, S_{rr}, of 32.3%, which was determined through the SWCC measured in laboratory water retentivity test and LG-A model [Mori et al., 2009]. Monthly average S_e is selected to determine monthly matric suction of base layer. Then, monthly representative E_2 is estimated with these monthly matric suction values. It is noted that S_r during freezing season is lower than residual S_r and S_e during freezing season is consequently lower than zero. This is due to functional features of the soil moisture sensor used in the measurement. For this reason, unrealistic measured low water content during freezing season is not used. The water content just before freezing is used as representative water content for freezing season.

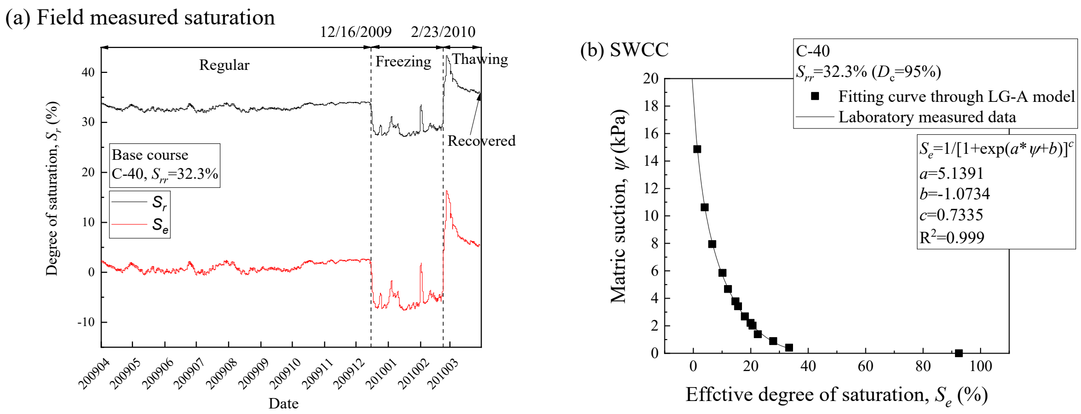

Fig. 6 (a) Long-term field measurement of base layer water content and (b) SWCC of C-40.

For subgrade layer, it is composed of Tomakomai soil. As the mechanical properties like resilient modulus of Tomakomai soil is under investigation and the test method of suction-controlled freeze-thaw MR test still needs verification, this study uses Toyoura sand, the standard test material, to verify newly developed test method and represent the subgrade material to check the climate effect on pavement life. It is assumed that effective degree of saturation, S_e, would be same in Toyoura sand subgrade and Tomakomai soil subgrade under same climate condition. S_e of subgrade layer illustrated as the red line in Fig. 7 (a) was calculated by using a residual degree of saturation (S_{rr}) of 25.67%, which was determined through the SWCC estimated with grain-size distribution of Tomakomai soil [Fredlund et al., 2002]. Consequently, monthly average S_e is selected to determine matric suction, ψ in Eq. (18), of subgrade layer in each month through laboratory measured SWCC of Toyoura sand and fitting curve through Fredlund-Xing model [Fredlund and Xing, 1994].

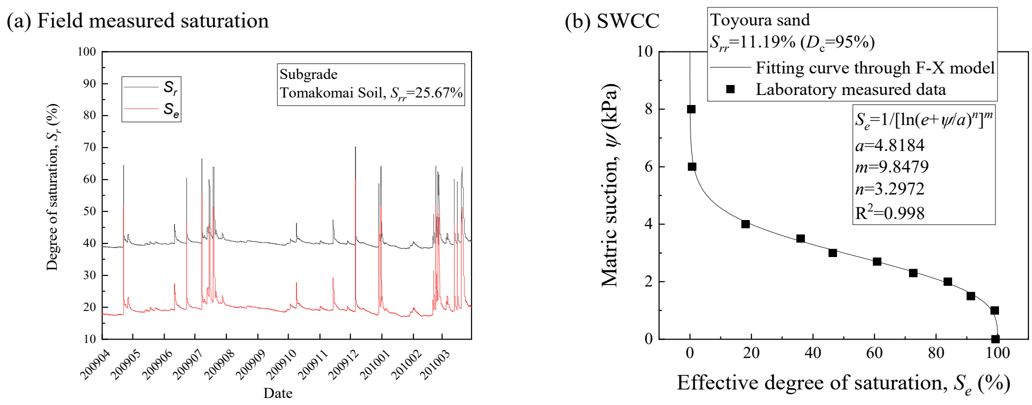

Fig. 7 (a) Long-term field measurement of subgrade layer water content and (b) SWCC of Toyoura sand.

The value of constants, k_1 to k_4, in Ng model (Eq. (18)) are determined through regression analysis on resilient modulus test results of C-40 and Toyoura sand with variant water contents. Resilient modulus of C-40 with three water contents, air-dried (S_r=8.2%), unsaturated (S_r=36.7%), saturated (S_r=100%), are determined through medium-size triaxial apparatus. More details about the apparatus and test procedure could be found in the previous study [Ishikawa et al., 2019a]. Resilient modulus of Toyoura sand with two water contents, unsaturated (S_r=40%), saturated (S_r=100%), are determined through freeze-thaw triaxial apparatus. More details about the apparatus and test procedure could be found in the previous study [Lin et al., 2020]. Consequently, Fig. 8 and 9 show the laboratory measured resilient modulus of C-40 and Toyoura sand and corresponding fitting surface through Ng model respectively. Table 1 summarized the value of constants, k_1 to k_4, in Ng model for C-40 and Toyoura sand.

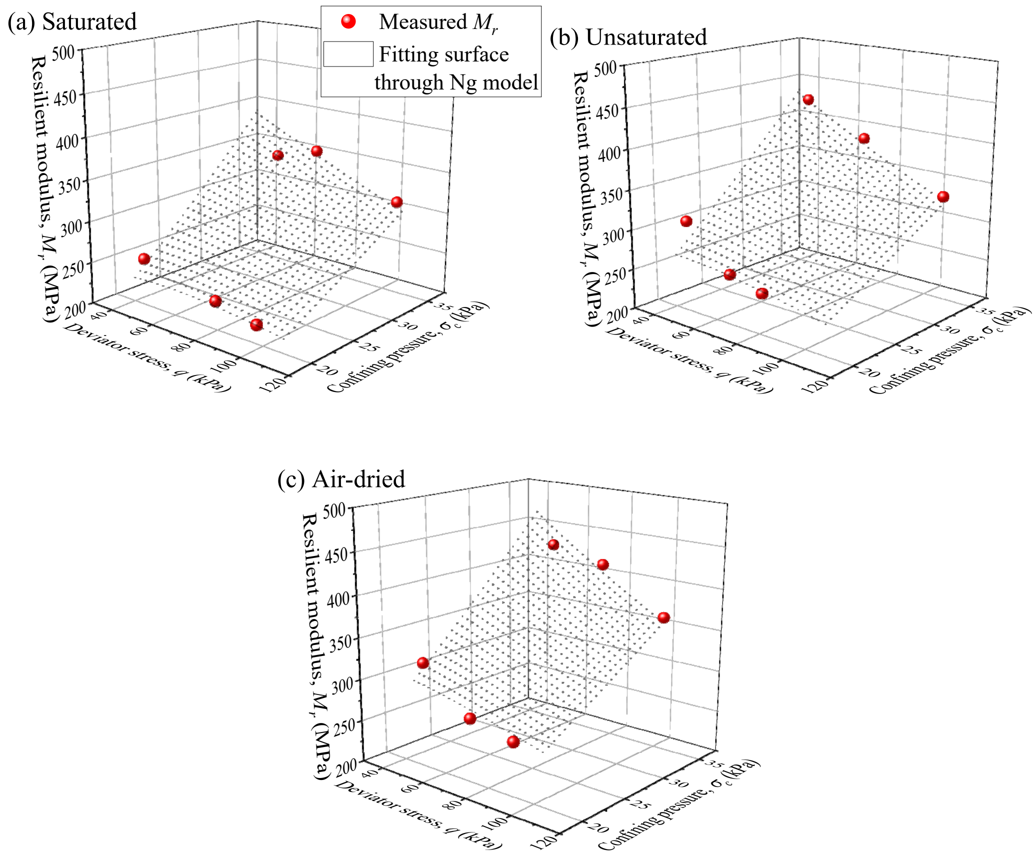

Fig. 8 Resilient modulus of C-40 under different water contents.

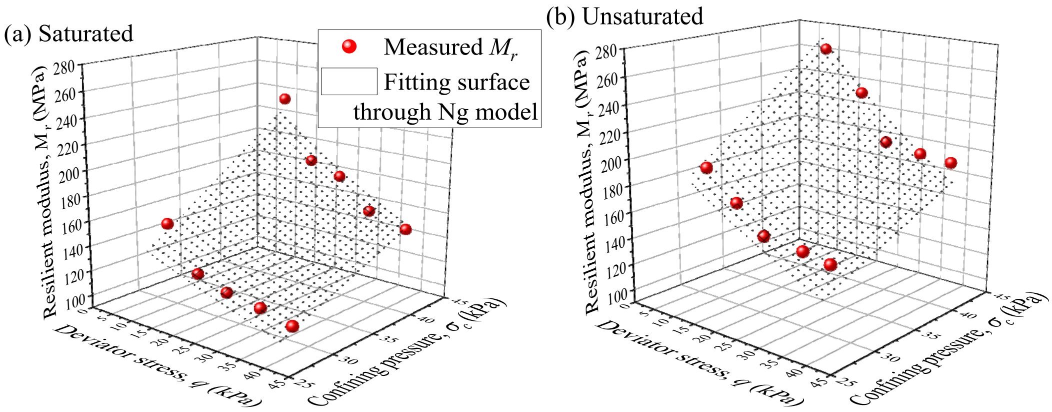

Fig. 9 Resilient modulus of Toyoura sand under different water contents.

Table 1. Value of regression constants.

	k_1	k_2	k_3	k_4	R^2
C-40	3.042	0.886	-1.696	1.076	0.939
Toyoura sand	2.103	1.065	-4.843	2.74	0.949

θ, τ_{oct}, and σ_{net} in Eq. (18) for base layer and subgrade layer are determined with a principal stress ratio equals to 4 under 10 and 5 kPa confining pressure respectively. It is noted that this stress condition was selected so that M_r at normal season matches layer stiffness determined in previous research [Maruyama et al., 2008]. Consequently, Table 2 shows the monthly representative base and subgrade layer moduli considering fluctuating water contents estimated through Ng model.

Table 2 Monthly representative layer moduli considering fluctuating water contents

Name	Elastic moduli (MPa)											
	Jan	Feb	Mar	Apr	May	Jun	Jul	Aug	Sep	Oct	Nov	Dec
Base layer, E_2	217	209	143	193	195	195	174	185	195	191	189	208
Subgrade layer, E_3	77	75	61	76	76	71	69	76	76	76	76	75

3.1.2 Freeze-thaw action

When considering the synergistic effect between freeze-thaw action and seasonal fluctuation in water content on the stiffness of base and subgrade layer, the monthly representative elastic moduli were divided into three types of seasonal E values (E for freezing season, thawing season, and regular season except for freezing and thawing seasons) for the simplicity of the pavement life analysis.

Since there is no freeze-thaw effect during the regular season, the E value for the regular season is estimated by Ng model as shown in Eq. (18) in a same way introduced in last section.

The E_2 and E_3 value for freezing season is set as 600 MPa and 200 MPa separately, according to back analysis of FWD test results [Ishikawa et al., 2019a]. In addition, this study assumes that when the average frost-penetration depth for the month gets into the base or subgrade layer regardless of deep or shallow, the E increases due to freezing. Here, the average frost-penetration depth (z) was calculated by substituting the freezing index calculated from the daily mean air temperatures measured by AMeDAS into the modified Berggren formula [Aldrich Jr, 1956] shown below:

$$z = \alpha\sqrt{\frac{172800F}{(L/\lambda)_{eff}}} \tag{19}$$

where α is a correction coefficient; F is a freezing index which is the average air temperature during freezing season multiplied by its duration in days; $(L/\lambda)_{eff}$ is an effective ratio of L to λ; L is the latent heat of soil; λ is a thermal conductivity of the soil.

The E value for thawing season stands for the average value between the moduli just after thawing, corresponds to the highest water content during thawing season, and the moduli at the end of thawing season, corresponds to the lowest water content during thawing season. The E value during thawing season is estimated by modified Ng model (Eq. (20)), which is proposed by Lin et al. [2020], with considering climate effect, F_{clim}. By adding new parameter F_{clim} into Ng model as shown in Eq. (20), modified Ng model captures the complex climate effect. The E value at the end of thawing season is estimated through Eq. (18) since the effect of freeze-thaw is excluded.

$$M_r = F_{clim} \cdot k_1 \cdot p_a \left(\frac{\theta}{p_a}\right)^{F_{clim} \cdot k_2} \left(\frac{\tau_{oct}}{p_a} + 1\right)^{F_{clim} \cdot k_3} \left(\frac{\psi}{\sigma_{net}} + 1\right)^{F_{clim} \cdot k_4} \tag{20}$$

Except modified Ng model, Liang model [Liang et al., 2008] is another approach to estimate resilient modulus with changing stress states like bulk stress, octahedral shear stress, and matric suction. Eqs (21) and (22) show the Liang model. The most difference between Liang model and Ng model is that the former one incorporates the matric suction into applied bulk stress, while the latter one extends the independent stress state variable. To capture the freeze-thaw effect on resilient modulus, Ishikawa et al. [2019a] modified Liang model (Eq. (23)) is built by adding a reduction factor, $f(N_f,\theta)$, on Eq. (21). $f(N_f,\theta)$ uses number of freeze-thaw process cycles (N_f) and volumetric water content (θ) for the sample as explanatory variables.

$$M_R = k_1 p_a \left(\frac{\theta_b+\chi\psi}{p_a}\right)^{k_2} \left(\frac{\tau_{oct}}{p_a}+1\right)^{k_3} \tag{21}$$

$$\chi = \left(\frac{(u_a-u_w)_b}{\psi}\right)^{0.55} \tag{22}$$

$$M_R = f\left(N_f,\theta\right) \cdot k_1 p_a \left(\frac{\theta_b+\chi\psi}{p_a}\right)^{k_2} \left(\frac{\tau_{oct}}{p_a}+1\right)^{k_3} \tag{23}$$

where θ_b is bulk stress; $(u_a\text{-}u_w)_b$ is air entry value.

For base course material, both Ng model (Eq. (18)) and Liang model (Eq. (21)) have high R^2 value on the unfrozen C-40 material as shown in Table 3. The applicability of modified Ng model (Eq. (20)) and modified Liang model (Eq. (23)) on freeze-thawed C-40 are checked by comparing estimated M_r with freeze-thawed $M_{r(\mathrm{CBR})}$. Freeze-thawed $M_{r(\mathrm{CBR})}$ is detected with a freeze-thaw CBR (California Bearing Ratio) test apparatus which is based on a general CBR test apparatus and improved to reproduce in a laboratory environment the freeze-thaw history expected to be applied to the base course materials in the in-situ pavement structures. A series of freeze-thaw CBR tests for C-40 was conducted under three different water contents, air-dried (S_r=12.3%), unsaturated (S_r=67%), saturated (S_r=95%), along with three different patterns of freeze-thaw history, no freeze-thaw, once freeze-thaw, and twice freeze-thaw, in order to examine the effects of freeze-thaw action and water content on the frost-heave and bearing-capacity characteristics of base course material. More details about the freeze-thaw CBR test apparatus and procedure could be found in the previous study [Ishikawa et al., 2019a]. Fig. 10 shows the $M_{r(\mathrm{CBR})}$ and estimated M_r with Eq. (20) and (23). It is noted that, both models can give reasonable predicted M_r and also capture the decreasing M_r with more freeze-thaw numbers and higher water contents. Table 3-1 also shows the R^2 value, F_{clim}, and $f(N_f,\theta)$ of modified Ng model (Eq. (20)) and modified Liang model (Eq. (23)) on freeze-thawed $M_{r(\mathrm{CBR})}$. It is noted that when conducting regression analysis for freeze-thawed test, only F_{clim} and $f(N_f,\theta)$ are variant and k_1 to k_4

are fixed to check the validity of newly added parameters. Both models show high accuracy (R^2>0.9).

Table 3. Applicability of Modified Liang model and Modified Ng model on C-40

		k_1	k_2	k_3	k_4	F_{clim}	$f(N_f,\theta)$	R^2
U	Ng model	3.042	0.886	-1.696	1.076	—	—	0.939
	Liang model	4.861	1.525	-2.092	—	—	—	0.950
FT	modified Ng model	3.042	0.886	-1.696	1.076	0.749	—	0.921
(N_f=1)	modified Liang model	4.861	1.525	-2.092	—	—	0.891	0.991
FT	modified Ng model	3.042	0.886	-1.696	1.076	0.644	—	0.968
(N_f=2)	modified Liang model	4.861	1.525	-2.092	—	—	0.800	0.998

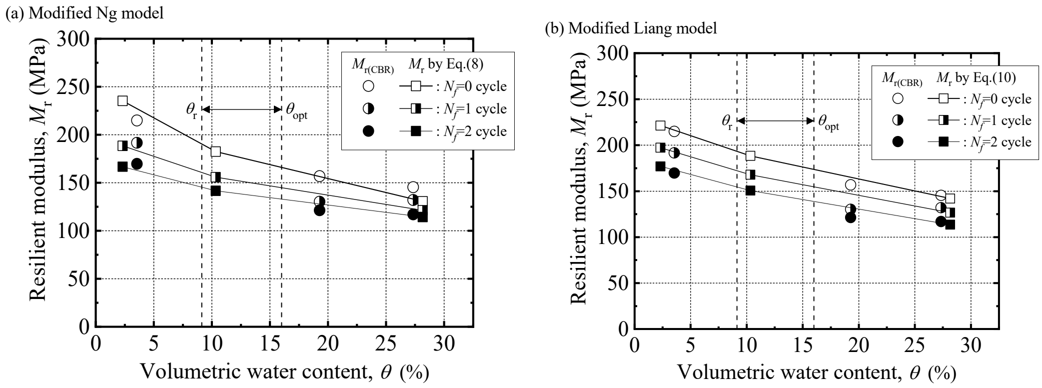

Fig. 10 Estimated M_r with (a) modified Ng model and (b) modified Liang model.

For subgrade material, Table 4 shows the applicability of Ng model (Eq. (18)) and Liang model (Eq. (21)) on unfrozen Toyoura sand, and the applicability of modified Ng model (Eq. (20)) and modified Liang model (Eq. (23)) on freeze-thawed Toyoura sand. Freeze-thaw resilient modulus of Toyoura sand is detected with freeze-thaw triaxial apparatus which could circulate low temperature fluids in the cap, pedestal, and inner cell to control the cap, pedestal, and around temperature of specimen separately to simulate one-dimensional freeze-thaw action. A series of freeze-thaw resilient modulus tests for Toyoura sand was conducted under two different water contents, unsaturated (S_r=40%), saturated (S_r=100%), along with two different patterns of freeze-thaw history, no freeze-thaw and once freeze-thaw, in order to examine the effects of freeze-thaw action and water content on the mechanical properties of subgrade materials. More details about the test condition and results could be found in previous research [Lin et al., 2020]. Fig. 11 shows the freeze-thaw resilient modulus test results for Toyoura sand. It is noted that unfrozen resilient modulus test results for Toyoura sand is already plotted in Fig. 9.

Table 4. Applicability of Modified Liang model and Modified Ng model on Toyoura sand

		k_1	k_2	k_3	k_4	F_{clim}	$f(N_f,\theta)$	R^2
U	Ng model	2.103	1.065	-4.843	2.74	—	—	0.949
	Liang model	2.396	0.979	-4.912	—	—	—	0.767
FT	modified Ng model	2.103	1.065	-4.843	2.74	0.885	—	0.901
(N_f=1)	modified Liang model	2.396	0.979	-4.912	—	—	0.910	0.621

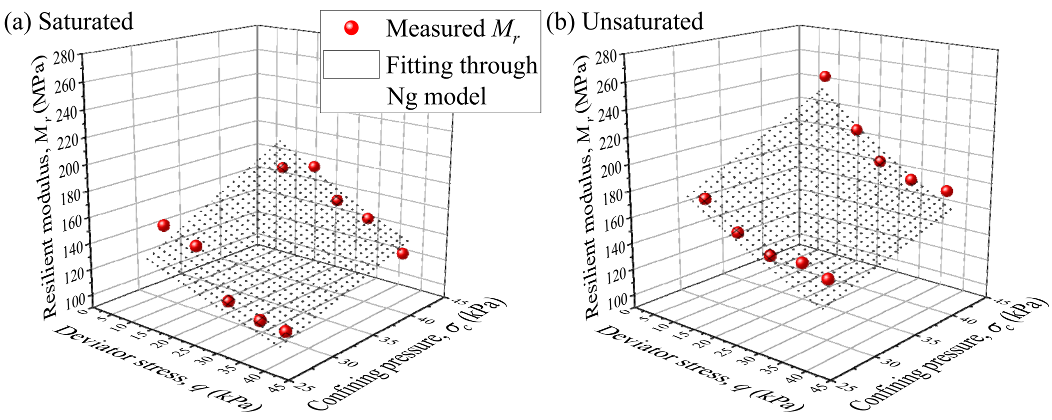

Fig. 11 Freeze-thaw resilient modulus of Toyoura sand under different water contents.

When performing regression analysis for freeze-thaw test results through modified Ng model (Eq. (10)) or modified Liang model (Eq. (12)), only F_{clim} and $f(N_f,\theta)$ are variant and k_1 to k_4 are fixed to the same value obtained from regression analysis on unfrozen test results to check the validity of newly added parameters. It is recognized that Ng model shows much higher R^2 value than Liang model no matter for unfrozen or freeze-thawed C-40 and Toyoura sand. Consequently, this study uses modified Ng model to estimate resilient modulus of base layer and subgrade layer with fluctuating water content and various freeze-thaw histories. In addition, Table 5 shows the monthly representative base and subgrade layer moduli estimated through modified Ng model with considering fluctuating water contents and freeze-thaw action. Through comparing Table 2 and 5, it is concluded the M_r increases to a high value during freezing season and drops further in thawing season according to the thaw weakening no matter for base or subgrade layer.

Table 5 Monthly representative layer moduli considering climate effect

Name	Elastic moduli (MPa)											
	Jan	Feb	Mar	Apr	May	Jun	Jul	Aug	Sep	Oct	Nov	Dec
Base layer, E_2	600	600	110	193	195	195	174	185	195	191	189	208
Subgrade layer, E_3	77	200	50	76	76	71	69	76	76	76	76	75

3.2 Dependency of resilient modulus on stress state

As discussed in introduction part, present Japanese design guide use constant elastic moduli of base layer and subgrade layer to calculate the strains under 49-kN wheel load. To overcome the limitation that unchangeable layer moduli under variant stress states caused by different layer thickness, the widely used resilient modulus in MEPDG, which changes with different stress states like deviator stress and confining pressure, is applied in this study to estimate the layer stiffness precisely. A convergence analysis of M_r is necessary to determine the reliable layer stiffness under 49-kN wheel loads since M_r affects and is conversely affected by the stress states. The convergence analysis is conducted through following steps [JSCE 2015]:

1) Input E_1, E_2^1, and E_3^1 in the GAMES to obtain the stress states in base layer and subgrade layer. According to previous researches [Huang, 2004], stress states in two points shown in Fig. 12 are chosen to estimate E for whole base and subgrade layer.

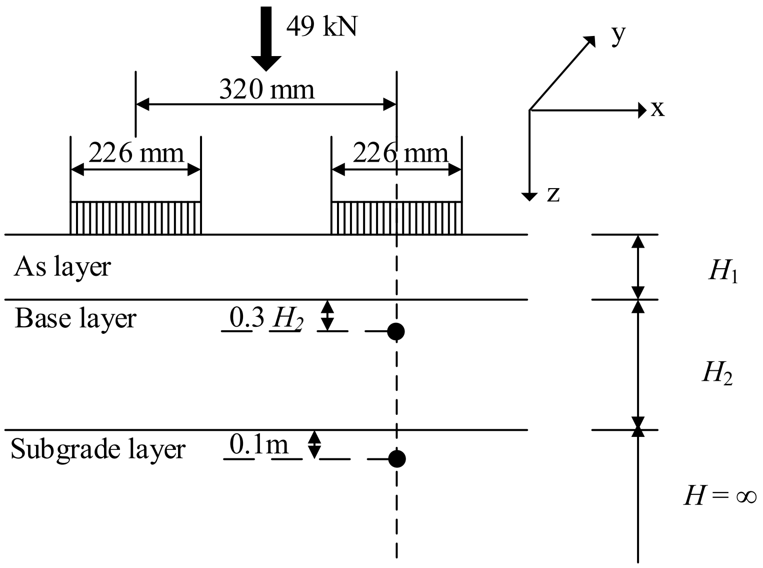

Fig. 12 Stress states calculation points in base and subgrade layer.

2) Substitute the stress states obtained in step 1 into modified Ng model to obtain new E_2^2 and E_3^2.

3) Step 1 and 2 are repeated until the error calculated in following equation is less than 1%.

$$e_{rr} = \frac{|E^{i-1} - E^{i}|}{E^{i}} \times 100 \tag{24}$$

where E^i and E^{i-1} is the layer modulus estimated in *i* th and *i*-1th iterations.

Based on this convergence analysis sequence, Fig. 13 shows the development of estimated resilient modulus of base layer and subgrade layer with number of iterations in normal season (Aug). It is noted that all moduli are stable after 2-4 iterations. Besides, convergent E_2 decreases in all pavement sections and convergent E_3 decreases in section A, B, C while increases in section D compared with elastic moduli without convergence analysis. Resilient moduli in other month show similar tendency that E_2 decreases in all pavement sections and E_3 decreases in section with thin As layer while increases in section with thick As layer.

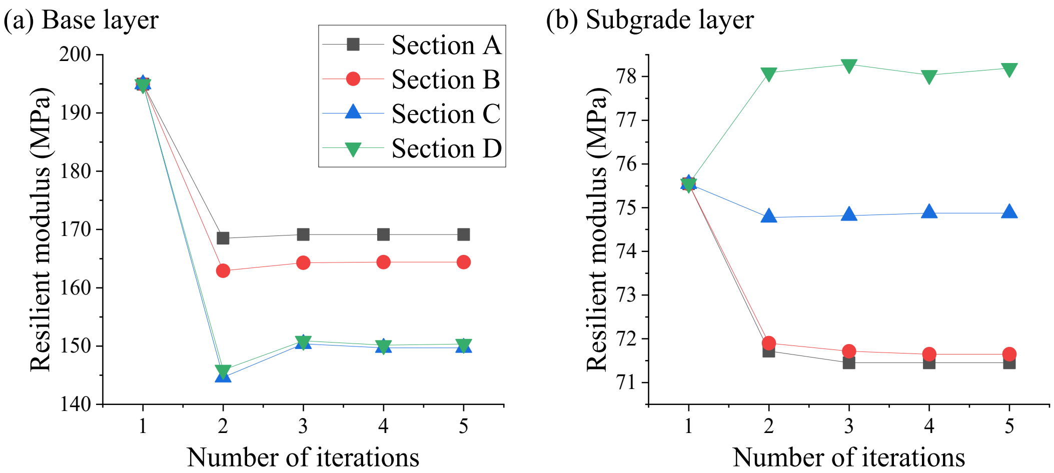

Fig. 13 Estimated resilient modulus of (a) base layer and (b) subgrade layer.

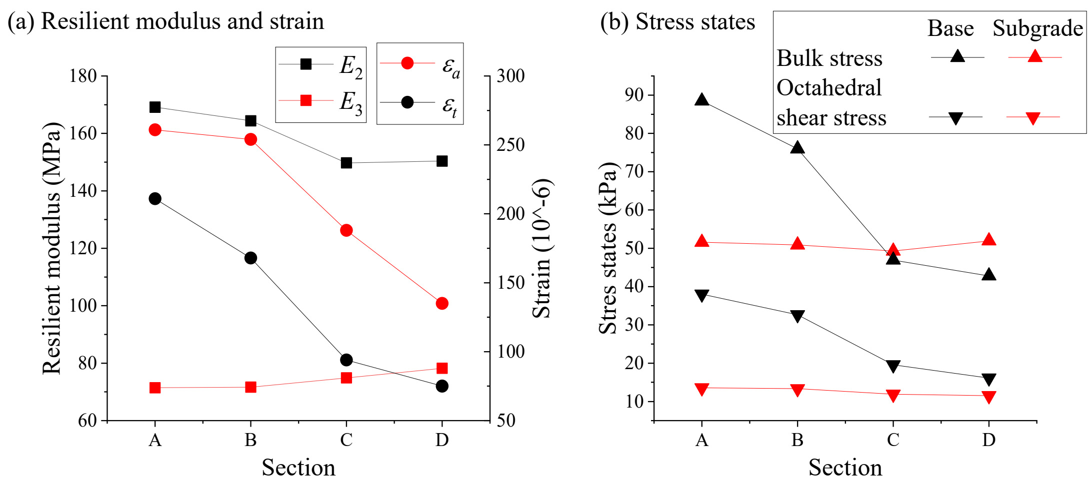

Fig. 14 (a) Resilient modulus and (b) stress states in different sections.

Different increasing or decreasing tendency comes from the variant stress states when pavement structures changing. To clearly discuss how pavement structures and stress states influence the resilient modulus at stable condition, Fig. 14 compares resilient modulus, strain, and stress states in different sections. Since As layer thickness increases from section A to D, it is concluded that E_2 decreases significantly with As layer thickness while E_3 slightly increases with As layer thickness. It is noted that Fig. 14 only show convergent resilient modulus and corresponding stress sates for Aug, which stands for the normal season, and that resilient modulus and corresponding stress sates for other months show the same tendency. Such tendency could be attributed to the changing bulk stress (θ) and octahedral shear stress (τ_{oct}) with As layer thickness, as shown in Fig 14 (b). θ has a positive effect on the M_r while τ_{oct} has a negative effect. In base layer, decreasing θ with thicker As layer is more significant than decreasing τ_{oct} with thicker As layer. Consequently, E_2 decreases from A to D. In subgrade layer, θ increases while τ_{oct} decreases with As layer thickness. As a result, E_3 increases from A to D. Since fluctuation of stress states in base layer is much significant than those in subgrade layer, fluctuation of moduli in base layer is accordingly larger. Elastic strains (ε_a and ε_t) are also shown in Fig. 14 (a). It is clear that no matter compressive strain (ε_a), which is used in Eq. (1) to calculate N_{fs}, or tensile strain (ε_t), which is used in Eq. (4) to calculate N_{fa}, both strains decrease with As layer thickness. Such tendency is reasonable as asphalt mixture has a much larger stiffness than crusher-run material and subgrade soil, and a thicker As layer improves the mechanical properties of the whole multi-layer elastic structure. Table 6 summarizes the convergent monthly representative base/subgrade layer moduli in A section. M_r for freezing season keeps constant due to freezing of soils. In this case, this study only performs the convergence analysis again M_r except the freezing season.

Table 6 Convergent monthly representative base/subgrade layer moduli in A section.

Name	Elastic moduli (MPa)											
	Jan	Feb	Mar	Apr	May	Jun	Jul	Aug	Sep	Oct	Nov	Dec
E_2-Water content fluctuation	191	185	132	173	175	175	161	169	176	172	170	184
E_2-Climate effect	600	600	105	173	175	175	161	169	176	172	170	184
E_3-Water content fluctuation	74	73	58	74	73	69	68	72	73	73	73	73
E_3-Climate effect	77	200	40	74	73	69	68	72	73	73	73	73

3.3 Influence of stress state and climate effect on pavement life

3.3.1 Stress state dependency

Fig.15 illustrates the calculated pavement life of all sections through layer moduli with and without convergence analysis. The ratio of N_f with convergent E_2 and E_3 to N_f without convergent E_2 and E_3 is also plotted here. Pavement life under water content fluctuation condition, which means layer stiffness E_2 and E_3 changing with water contents, and climate condition, which means E_2 and E_3 changing with water contents and freeze-thaw action, are shown in Figs.15 (a) and (b) separately. N_{fa} always decreases with convergent E_2 and E_3 regardless of pavement structures while N_{fs} only decreases with convergent E_2 and E_3 in pavement structures with thin As layer (A, B, T1 and T2). Convergent E_2 and E_3 has a negative effect on the pavement life against fatigue cracking and this effect is more significant in thick As layer pavement structure. On the other hand, convergent E_2 and E_3 has a negative effect on the pavement life against rutting when As layer is thin. Consequently, convergence analysis for layer stiffness is essential when developing a mathematical flexible pavement design method with high applicability and precision.

In addition, the effect of convergence analysis on pavement life is basically more significant compared with effect of water content fluctuation or climate effect regardless of section structure. To be precise, the difference between N_f-Original, the pavement life calculated with constant E_2 and E_3, and N_f-without convergence is less significant than the difference between N_f-without convergence and N_f-with convergence no matter the water content fluctuation (Fig. 15(a)) or climate effect is considered (Fig. 15(b)). The only exception that the effect of convergence analysis is less significant than effect of water content fluctuation or climate effect is for the pavement life against rutting (N_{fs}) of structure with thick As layer. For example, for section C and D, the difference between N_{fs}-Original and N_{fs}-without convergence is more significant than the difference between N_{fs}- without convergence and N_{fs}-with convergence. Such results indicate that in pavement structures such as high-standard roads, environmental condition dependence has a greater effect on pavement life than stress dependence and should be considered as a more significant factor. Especially in the case of Japanese pavement where rutting is more of a problem than fatigue cracking.

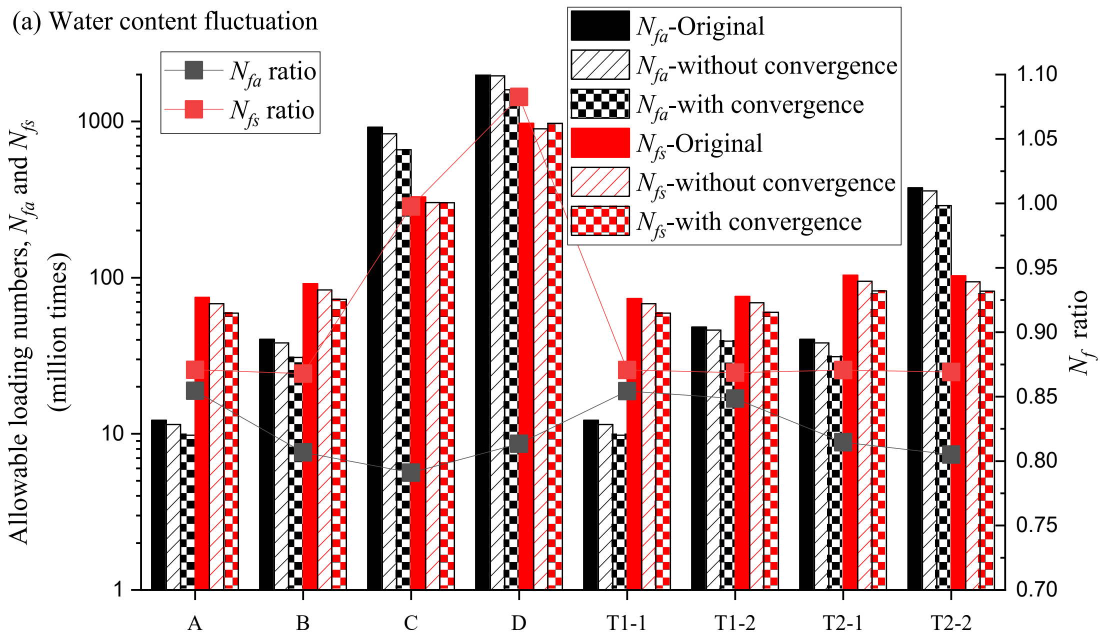

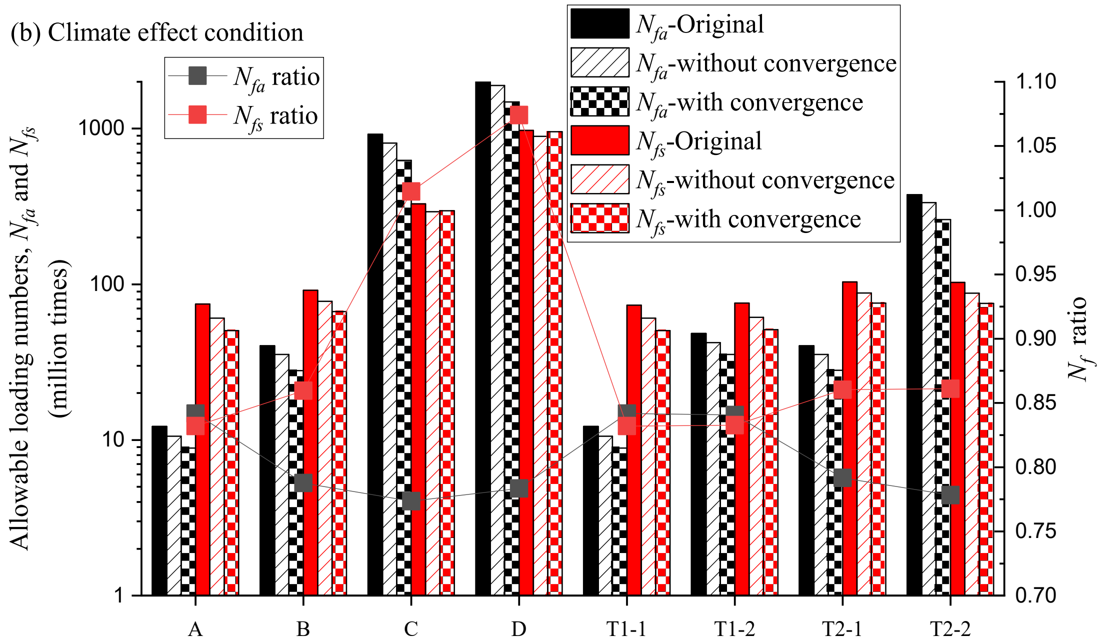

Fig. 15 Convergence analysis effect on pavement life under (a) water content fluctuation condition (b) climate effect condition

3.3.2 Climate effect on pavement life

Figs. 16 and 17 illustrate N_{fs} and N_{fa} of eight test pavement structures under three conditions, namely Original, Water content fluctuation, and Climate effect. It is noted that all pavement life in water content fluctuation condition and climate condition are calculated with convergent layer moduli. In other words, Figs. 16, 17 are plotted by rearranging the calculation results in Fig. 15. It is obvious that N_{fs} and N_{fa} both decrease from original condition to water content condition, which implies that changing E_2 and E_3 with fluctuating water content decrease pavement life. N_{fs} and N_{fa} decrease further from water content fluctuation condition to climate condition, which indicates that freeze-thaw action decreases pavement life further as the decreasing E_2 and E_3 during thawing season has a stronger influence on the pavement life than the increasing E_2 and E_3 during the freezing season.

To clearly discuss the influence of water content fluctuation, freeze-thaw action, and climate effect on the pavement life, R_{Nf} for different structures are also plotted in the Figs. 16 and 17. The R_{Nf} considering water content fluctuation or climate effect are determined through dividing the N_f-Water content fluctuation or N_f-Climate effect by the N_f-Original, while the R_{Nf} considering freeze-thaw action is determined through dividing the N_f-Climate effect by the N_f-Water content fluctuation. All ratios are lower than 1, indicates that influence of water content fluctuation, freeze-thaw action, and climate effect on E_2 and E_3 all decrease the pavement life. Within pavement life against rutting calculation results, R_{Nf} caused by water content, freeze-thaw action, and climate effect are around 0.819, 0.931, and 0.765 separately. In other words, the N_{fs} decreases 18.1% when changing E_2 and E_3 caused by water content fluctuation is considered and it would further decrease 6.9% when effect of freeze-thaw action on E_2 and E_3 is also considered. A synergistic climate effect on E_2 and E_3 decreases N_{fs} about 23.5%. Within pavement life against fatigue cracking calculation results, R_{Nf} caused by water content, freeze-thaw action, and climate effect are around 0.759, 0.93, and 0.706 separately. In other words, the N_{fa} decreases 24.1% when changing E_2 and E_3 caused by water content fluctuation is considered and it would further decrease 7% when effect of freeze-thaw action on E_2 and E_3 is also considered. A synergistic climate effect on E_2 and E_3 decreases N_{fa} about 29.4%. It is noted that, all these decreasing ratios include the effect of convergence analysis discussed in previous section.

These results suggest that for improving the applicability and validity of the current Japanese design standard, the introduction of the theoretical design method for pavement structures, which can take account of the effects of the freeze-thaw actions and the concurrent seasonal fluctuation in water content on the base and subgrade layer stiffness, is effective in the asphalt pavements for cold regions.

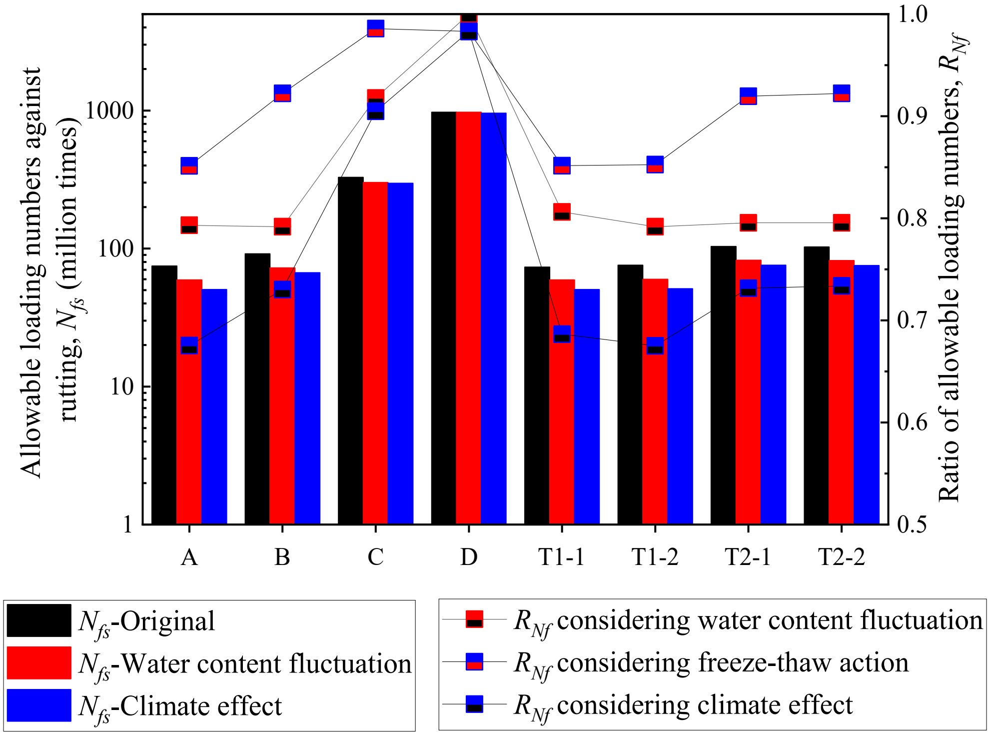

Fig. 16 N_{fs} of eight test pavement structures.

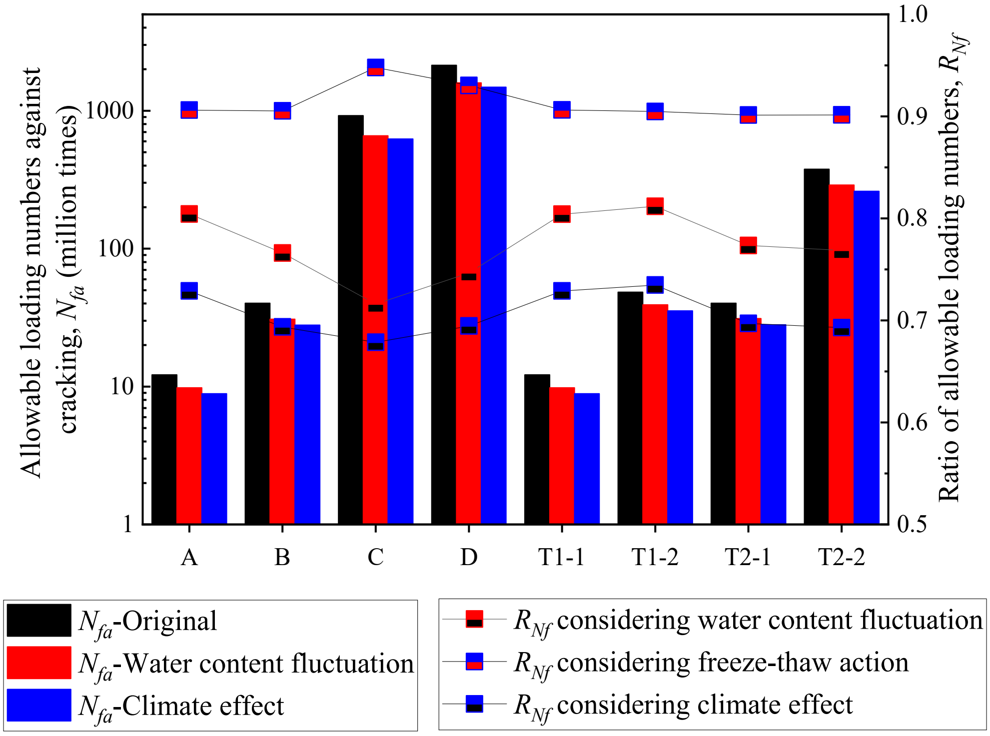

Fig. 17 N_{fa} of eight test pavement structures.

4. Modification of failure criteria

4.1 MEPDG rutting prediction model

To overcome the limitations of Japanese rutting failure criterion explained in the introduction part, this section modified the structure of AI model (Eq. (3)) referring to MEPDG rutting depth prediction model (Eq. (2)).

By applying the rutting failure threshold value in present Japanese design guide (15mm) into Eq. (2), allowable loading number against rutting could be calculated through Eq. (25).

$$N_{fs} = \rho \cdot \left(ln\left(\frac{\beta_{s1} k_1 \varepsilon_v h\left(\frac{\varepsilon_0}{\varepsilon_r}\right)}{15} \right) \right)^{-1/\beta} \quad (25)$$

Fig. 18 shows the allowable loading number against rutting through AI model (namely N_{fs},-AI) and MEPDG model (namely N_{fs},-MEPDG) under various elastic compressive strain (ε_v). N_{fs}-AI is much larger than N_{fs}-MEPDG when ε_a locates between 50 to 500 E-6, which is the normal range for ε_a. In other words, AI model greatly overestimate the allowable loading number against rutting as compared with MEPDG model. To modify the AI model based on MEPDG, this study introduces an adjusting parameter, β_m, to the traditional AI model. Newly developed one is named as AI-MEPDG rutting model as show in Eq. (26). β_m is calculated through dividing N_{fs}-MEPDG by N_{fs}-AI. A logistic function is used to build the relation between β_m and ε_a, as shown in Fig. 18 and Eq. (27). Consequently, AI-MEPDG rutting model is shown in Eqs. (26) and (27) to calculate allowable loading number against rutting.

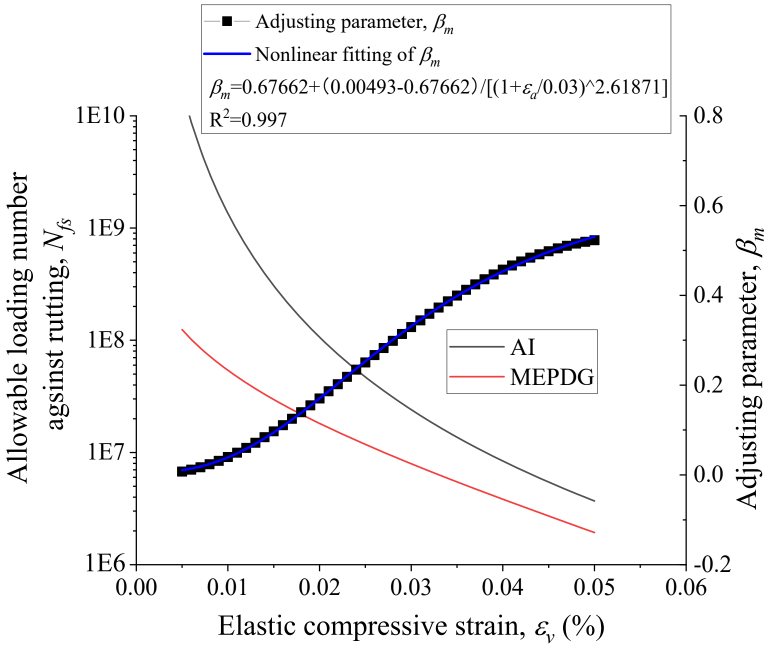

Fig. 18 Allowable loading number against rutting calculated through AI and MEPDG model.

$$N_{fs} = \beta_m \cdot \beta_{s1} \cdot \{1.365 \times 10^{-9} \cdot \varepsilon_a{}^{-4.477 \cdot \beta_{s2}}\} \tag{26}$$

$$\beta_m = A_2 + \frac{A_1 - A_2}{1+(\varepsilon_a/x_0)^p} \tag{27}$$

A_1 and A_2: lower and upper limit of β_m and the A_1 is forced as positive value. A_1=0.000493; A_2=0.67672.

x_0: fitting parameter, equals to 0.03.

p: fitting parameter, equals to 2.61871.

With AI-MEPDG rutting model, the N_{fs} in climate condition is calculated and illustrated in Fig. 19. It is noted that, N_{fs} through AI-MEPDG rutting model in Fig. 19 is calculated with convergent layer moduli. The tendency for the ratio of N_{fs} with convergence to N_{fs} without convergence in AI-MEPDG rutting model is almost similar to that in Fig. 15. AI-MEPDG rutting model gives much smaller predicted N_{fs} than AI model predicted value. However, compared with actual measured loading number at failure, predicted N_{fs} through AI-MEPDG rutting model are still too large. Bias between predicted and actual pavement life are probably caused by enormous variability between designed and actual geography, climatic conditions, construction materials, construction practices, traffic compositions and volumes. The cause for the bias should be examined in the next section.

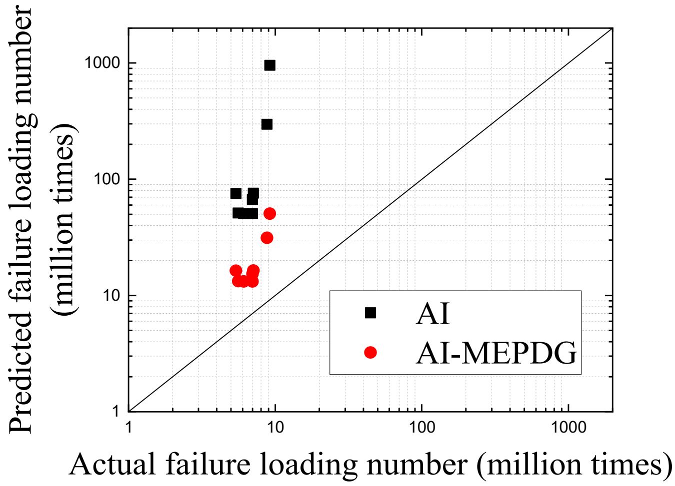

Fig. 19. Predicted N_{fs} and actual measured loading number at failure.

4.2 Principal stress axis rotation

As discussed before, the principal stress axis rotation (PSAR) is not considered in MEPDG, but seriously affects rutting depth. Including such phenomenon into rutting model helps removing bias and increasing the reliability. The amplified permanent strain caused by PSAR is examined by test results through multi-ring shear apparatus, which could simultaneously apply axial load and shear stress to simulate PSAR. More details about the multi-ring shear apparatus could be found at previous researches [Ishikawa et al., 2011]. Fig. 20 displays permanent axial strain of Toyoura sand with PSAR (hereafter is referred as Moving-wheel Loading test, ML test) and without PSAR (hereafter is referred as Fixed-point Loading test, FL test). Table 7 summarizes the experimental conditions of multi-ring shear tests.

Table 7 Experimental conditions of multi-ring shear tests.

Test	Test	Water	Specimen	Dry	Maximum	Maximum

Name	sample	content	Height (mm)	density (g/cm^3)	axial stress, $(\sigma_a)_{max}$ (kPa)	shear stress, $(\tau_{a\theta})_{max}$ (kPa)
FL	Toyoura sand	Oven-dried	100	1.463	72.58	0
FL	Toyoura sand	S_r=25.6%	100	1.463	72.58	0
FL	Toyoura sand	S_r=31.6%	100	1.463	72.58	0
FL	Toyoura sand	S_r=46%	100	1.463	72.58	0
ML	Toyoura sand	Oven-dried	100	1.463	72.58	18.12
ML	Toyoura sand	S_r=25.6%	100	1.463	72.58	18.12
ML	Toyoura sand	S_r=31.6%	100	1.463	72.58	18.12
ML	Toyoura sand	S_r=46%	100	1.463	72.58	18.12

It is obvious that PSAR greatly amplifies the permanent axial strain regardless of water content. To quantitatively describe the amplificated axial strain caused by PSAR, ratio of axial strain, $(R_s)_{ave}$, is also plotted in Fig. 20. $(R_s)_{ave}$ is determined through dividing permanent axial strain with PSAR to that without PSAR. Consequently, all ratios are stable around 1.90 after 180 loading cycles. According to previous research [Ishikawa et al., 2019b, Lin et al., 2019a], $(R_s)_{ave}$ could be roughly approximated by Eq. (28). In this case, the constant β_{PSAR} in Eq. (28) is determined as 2.57 according to the test results that $(R_s)_{ave}$ equals to 1.9, $(\sigma_a)_{max}$ and $(\tau_{a\theta})_{max}$ are 72.58 kPa and 18.12 kPa respectively.

$$(R_s)_{ave} = \exp\left(\beta_{PSAR}\frac{(\tau_{a\theta})_{max}}{(\sigma_a)_{max}}\right) \quad (28)$$

where $(\sigma_a)_{max}$ is maximum axial stress; $(\tau_{a\theta})_{max}$ is maximum shear stress; β_{PSAR} is material constant.

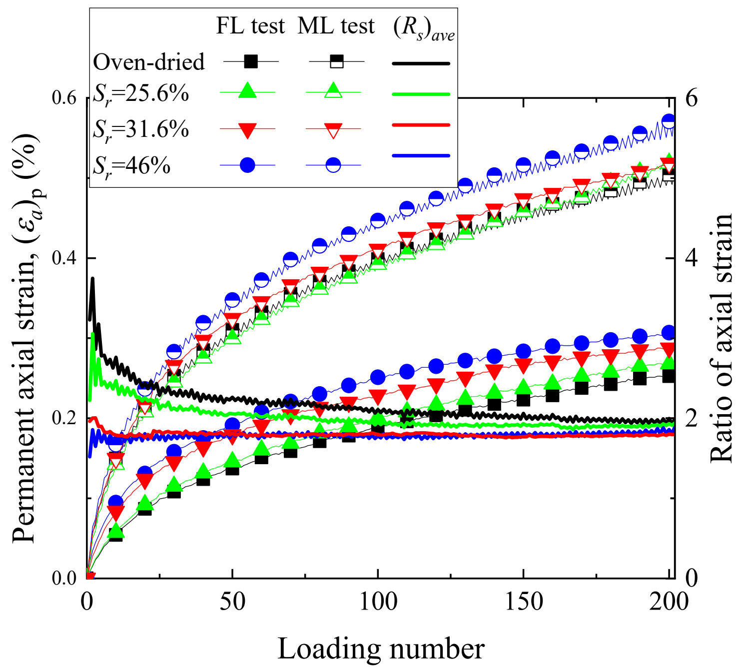

Fig. 20. Permanent axial strain of Toyoura sand.

As $(R_s)_{ave}$ represents the amplification of permanent axial strain caused by PSAR, the reciprocal of $(R_s)_{ave}$ represents the decreasing rate of failure loading number. As a result, Eq. (26) is modified by adding the reciprocal of $(R_s)_{ave}$ to capture the effect of PSAR on pavement life against rutting as shown in Eq. (29). It is noted that $(\sigma_a)_{max}$ and $(\tau_{a\theta})_{max}$ are stress states in laboratory test through multi-ring shear apparatus, and they are equal to vertical stress, $(\sigma_z)_{max}$, and shear stress, $(\tau_{yz})_{max}$, used in GAMES software.

$$N_{fs} = \beta_m \cdot \beta_{s1} \cdot \{1.365 \times 10^{-9} \cdot \varepsilon_a{}^{-4.477 \cdot \beta_{s2}}\}/\exp\left(\beta_{PSAR} \frac{(\tau_{yz})_{max}}{(\sigma_z)_{max}}\right) \quad (29)$$

To apply Eq. (29) into pavement life prediction, it is necessary to determining the suitable position in subgrade layer to estimate the $(\sigma_z)_{max}$ and $(\tau_{yz})_{max}$ through GAMES. To investigate how $(\sigma_z)_{max}$ and $(\tau_{yz})_{max}$ change with depth, Section A and layer moduli in Aug are chosen to build a model as shown in Fig. 21. As a consequence, Fig. 22 illustrates the σ_z and τ_{yz} in different depth, z, and corresponding $(R_s)_{ave}$. It is obvious that σ_z and τ_{yz} show same tendency regardless of h. σ_z reaches the largest value just below the wheel loading (y=0) and decreases with y. On the other hands, τ_{yz} is zero just below the wheel loading and increases to the largest value at y=600mm then decreases. When the z increases, both $(\sigma_z)_{max}$ and $(\tau_{yz})_{max}$ decreases. $(R_s)_{ave}$ in all conditions are around 2.1. Consequently, it is suggested to set the h as 10cm, same depth in convergent analysis of E_3 as shown in Fig. 12.

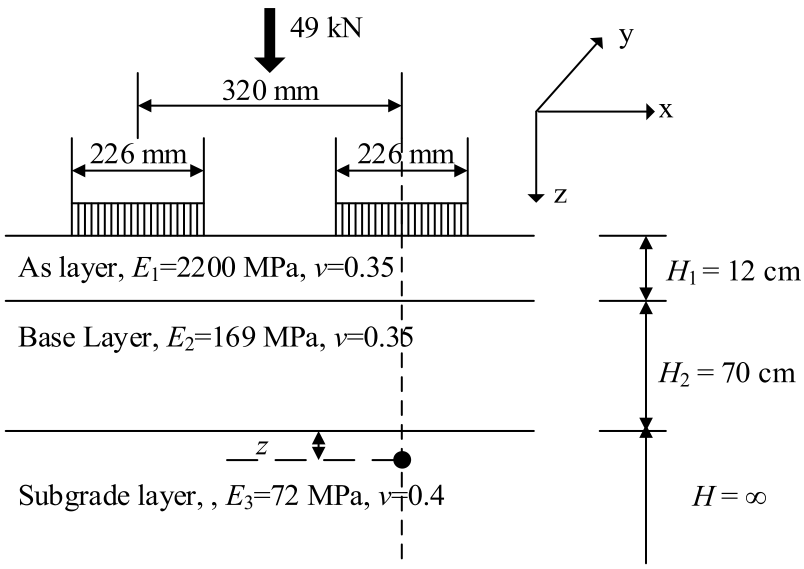

Fig. 21 Stress states calculation point in subgrade layer.

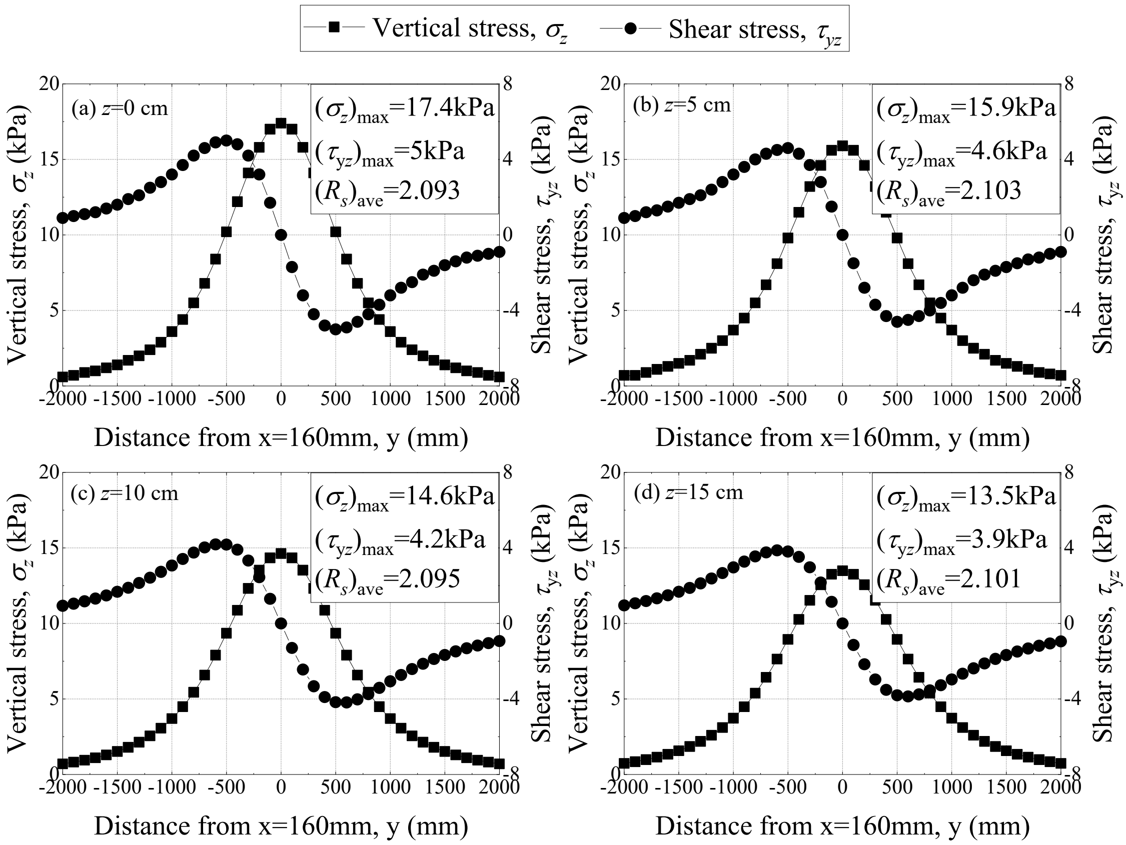

Fig. 22 σ_z and τ_{yz} in different depth and corresponding $(R_s)_{ave}$.

Allowable loading number against rutting failure calculated through Eq. (29) in all eight sections are shown in Fig. 23. It is obvious that PSAR greatly decreases calculated pavement life and N_{fs} with considering PSAR is most close to actual measured failure loading number. It is concluded the finally modified rutting model, AI-MEPDG-PSAR model, is useful and reliable to predict the allowable loading number against rutting of flexible pavements especially for roads located in cold regions like Hokkaido.

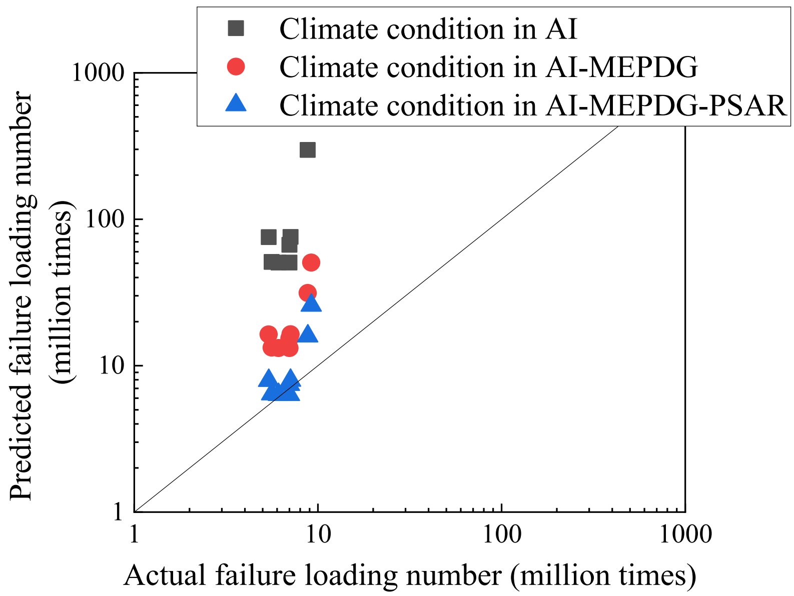

Fig. 23 Predicted N_{fs} considering PSAR.

Finally, the Fig. 24 illustrates the sequence in modified Japanese flexible pavement design guide. It should be noted that the modification achieved in this study specially focused on the base/subgrade layer mechanical properties and the rutting failure criterion as shown in the comparison between Fig. 24 and Fig. 2.

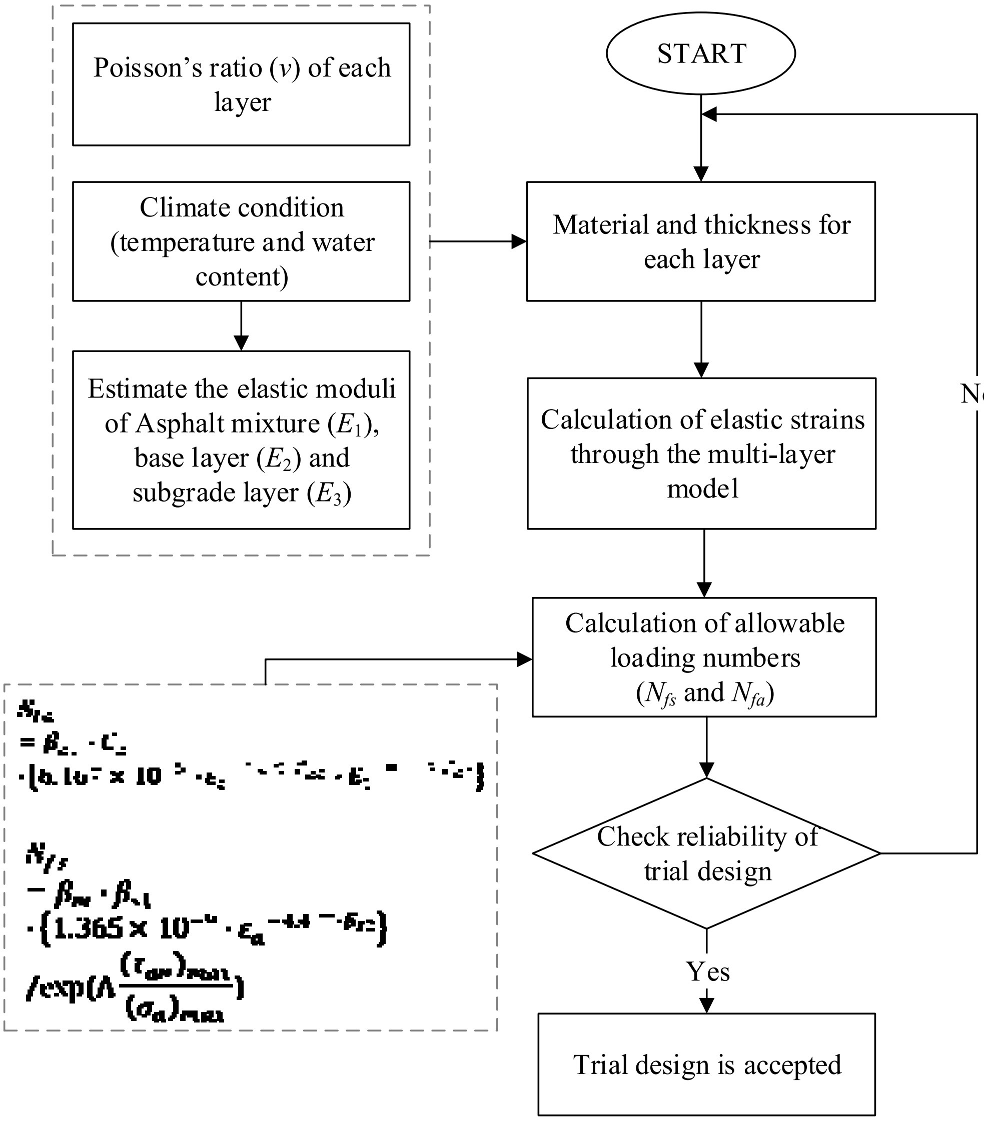

Fig. 24 Sequence in modified Japanese flexible pavement design guide.

5. Conclusions

The following findings can be mainly obtained:

- To modify current Japanese design guide by replacing constant subgrade layer moduli with a variant relating to water content fluctuation and freeze-thaw history, newly proposed modified Ng model, long-term measured in-situ base and subgrade layer water content, and laboratory obtained SWCC are used. Calculated pavement life against rutting and fatigue cracking proves that both water content fluctuation and freeze-thaw action degrade stiffness of base and subgrade layer and finally decrease the pavement life of asphalt pavements in cold regions.

- Convergence calculation are essential since the rigidity changes with pavement structures even if the influence of environmental conditions is taken into consideration. Environmental condition dependence has a greater effect on pavement life in pavement structures such as high-standard roads, especially in the case of Japanese pavement where pavement life against rutting is more of a problem than fatigue cracking.
- Principal stress axis rotation greatly amplifies the permanent strain compared with triaxial repeated loading test usually without such stress states. Ratio of axial strain, $(R_s)_{ave}$, is used to quantitatively describe the amplificated axial strain caused by principal stress axis rotation and added into rutting failure criterion to help increasing prediction accuracy and applicability.

These findings indicate that a detailed understanding of the mechanical behavior of the base and subgrade layer with complex water content fluctuation, freeze-thaw history, and stress states is essential to develop a mathematical model for the mechanical response of the base and subgrade layer in cold regions, and incorporate it into the theoretical design method for pavement structures. Besides, a modification on the structure of failure prediction model by considering principal stress axis rotation is also important to improve the prediction accuracy and applicability of mechanical-empirical design method for pavement in cold regions. Convergence analysis is recommended for users of proposed modified design method according to its effect on resilient modulus since the incorporation of all the improvements mentioned in this study into a program for pavement design and lifetime prediction could overcome the cumbersome calculations caused during the convergence analysis. Further and more comprehensive studies including more test on unbound granular materials with various water contents, local calibration with more tests pavements are recommended to examine the validity, limitation of application, and so forth as these findings are obtained through limited experimental conditions and only examined with some local test pavement projects.

Acknowledgements

This research was supported in part by Grant-in-Aid for Scientific Research (B) (20360206), (C) (15K06214), and (A) (16H02360) from Japan Society for the Promotion of Science (JSPS) KA-KENHI. Support from China Scholarship Council is also highly acknowledged.

References

[1] AASHTO 2008. Mechanistic-Empirical Pavement Design Guide: A Manual of Practice, Washington.

[2] Aldrich HP. Frost penetration below highway and air-field pavement. Highw Res Board Bull 1956;135:124-49.

[3] Asphalt Institute 1982. Research and Development of Asphalt Institute's Thickness Design Manual, 9th ed. Asphalt Institute, College Park Md.

[4] ASTM, 2011, Standard Practice for Classification of Soils for Engineering Purposes (Unified Soil Classification System) (D2487-11)

[5] Berg RL, Bigl SR, Stark JA, Durell GD. Resilient modulus testing of materials from Mn/Road: phase 1. 1996. https://doi.org/10.21949/1404573

[6] Brown SF. Soil mechanics in pavement engineering. Géotechnique 1996;46(3):383-426. https://doi.org/10.1680/geot.1996.46.3.383

[7] Cary CE, Zapata CE. Resilient modulus for unsaturated unbound materials. Road Mater Pavement Des 2011;12(3):615–38. https://doi.org/10.1080/14680629.2011.9695263

[8] Clayton CRI. Stiffness at small strain: research and practice. Geotech 2011;61:5-37. https://doi.org/10.1680/geot.2011.61.1.5

[9] Cole DM, Irwin LH, Johnson TC. Effect of freezing and thawing on resilient modulus of a granular soil exhibiting nonlinear behavior. Transp Res Rec J Transp Res Board 1981;809:19-26.

[10] Fredlund DG, Xing A. Equations for the soil-water characteristic curve. Can Geotech J 1994;31(4):521-532. https://doi.org/10.1139/t94-061

[11] Fredlund MD, Wilson GW, Fredlund DG. Use of the grain-size distribution for estimation of the soil-water characteristic curve. Can Geotech J 2002;39(5):1103-1117. https://doi.org/10.1139/t02-049

[12] Gräbe PJ, Clayton CR. Effects of principal stress rotation on permanent deformation in rail track foundations. J Geotech Geoenviron Eng 2009;135(4):555-565. https://doi.org/10.1061/(ASCE)1090-0241(2009)135:4(555)

[13] Han Z, Vanapalli SK. State-of-the-art: Prediction of resilient modulus of unsaturated subgrade soils. Int J Geomech 2016;16(4):04015104. https://doi.org/10.1061/(ASCE)GM.1943-5622.0000631

[14] Huang YH, 2004. Pavement Analysis and Design, 2nd ed. Pearson Education, Inc.

[15] Inam A, Ishikawa T, Miura S. Effect of principal stress axis rotation on cyclic plastic

deformation characteristics of unsaturated base course material. Soils Found 2012;52(3):465-480. https://doi.org/10.1016/j.sandf.2012.05.006

[16] Ishikawa T, Sekine E, Miura S. Cyclic deformation of granular material subjected to moving-wheel loads. Can Geotech J 2011;48(5):691-703. https://doi.org/10.1139/t10-099

[17] Ishikawa T, Lin T, Kawabata S, Kameyama S, Tokoro T. Effect evaluation of freeze-thaw on resilient modulus of unsaturated granular base course material in pavement. Transp Geotech 2019a;21:100284. https://doi.org/10.1016/j.trgeo.2019.100284

[18] Ishikawa T, Lin T, Yang J, Tokoro T, Tutumluer E. Application of the UIUC model for predicting ballast settlement to unsaturated ballasts under moving wheel loads. Transp Geotech 2019b;18:149-162. https://doi.org/10.1016/j.trgeo.2018.12.003

[19] Japan Meteorological Agency, Automated Meteorological Data Acquisition System. https://www.jma.go.jp/jp/amedas/

[20] Japan Society of Civil Engineers, 2015. Characteristics and Evaluation of Subgrade and Base Course Materials, Japan Society of Civil Engineers, Tokyo. [in Japanese]

[21] Japan Road Association, 2006. Pavement design manual, Japan Road Association, Tokyo. [in Japanese]

[22] Johnson TC, Cole DM, Chamberlain EJ. Influence of freezing and thawing on the resilient properties of a silt soil beneath an asphalt concrete pavement. U.S. Cold Regions Research and Engineering Laboratory, CRREL Report 78-23. 1978. http://hdl.handle.net/11681/9380

[23] Liang RY, Rabab'ah S, Khasawneh M. Predicting moisture-dependent resilient modulus

of cohesive soils using soil suction concept. J Transp Eng 2008;134(1):34-40. https://doi.org/10.1061/(ASCE)0733-947X(2008)134:1(34)

[24] Lin T, Ishikawa T, Yang J, Tokoro T. Evaluation of climate effect on resilient modulus of granular subgrade material, Cold Reg Sci Technol 2020. (under review)

[25] Lin T, Ishikawa T, Luo B. Applicability of modified University of Illinois at Urbana–Champaign model for unbound aggregate material with different water content, Transp Res Rec 2019a;2673(3):439-449. https://doi.org/10.1177/0361198119827530

[26] Lin T, Ishikawa T, Tokoro T. Testing method for resilient properties of unsaturated unbound granular materials subjected to freeze-thaw action. Japanese Geotech Soc Spec Publ 2019b;7(2):576-581. https://doi.org/10.3208/jgssp.v07.089

[27] Maina JW, Matsui K. Developing software for elastic analysis of pavement structure responses to vertical and horizontal surface loadings. Transp Res Rec J Transp Res Board 2004;1896(1):107-118. https://doi.org/10.3141/1896-11

[28] Maruyama K, Tako J, Kasahara A. Long-term performance of asphalt pavements at bibi new test road. J JSCE E 2006;62(3):519-530. [in Japanese] https://doi.org/10.2208/jsceje.62.519

[29] Maruyama K, Tako J, Kasahara A. Fatigue failure life prediction method of asphalt pavement. J JSCE E 2008;64(3):416-426. [in Japanese] https://doi.org/10.2208/jsceje.64.416

[30] Miura K, Miura S, Toki S. Deformation behavior of anisotropic dense sand under principal stress axis rotation. J Soils Found 1986;26(1):36-52. https://doi.org/10.3208/sandf1972.26.36

[31] Mori T, Kamiya K, Chiba T, Uzuoka R, Kazama M. The functional model of the soil-water characteristic curve used the logistic function during cyclic shearing. 44th Japan national conference on geotechnical engineering, Proc dom conf. 2009. p.1519-20. in Japanese.

[32] NCHRP 2004. Guide for mechanistic-empirical design of new and rehabilitated pavement structures.

[33] Ng CWW, Zhou C, Yuan Q, Xu J. Resilient modulus of unsaturated subgrade soil: experimental and theoretical investigations. Can Geotech J 2013;50(2):223-232. https://doi.org/10.1139/cgj-2012-0052

[34] Seed HB, CHAN CK, Monismith CL. Effects of repeated loading on the strength and deformation of compacted clay. Highw Res Board Proc 1955;34:541-558.

[35] Simonsen E, Janoo VC, Icacsson U. Resilient properties of unbound road materials during seasonal frost conditions. J Cold Reg Eng 2002;16(1):28–50. https://doi.org/10.1061/(ASCE)0887-381X(2002)16:1(28)

[36] Simonsen E, Isacsson U. Soil behavior during freezing and thawing using variable and constant confining pressure triaxial tests. Can Geotech J 2001;38(4):863-875. https://doi.org/10.1139/t01-007